
QUANTUM-ELECTRODYNAMIC PROCESSES NEAR THE SURFACE

QED-Modified Radiative Properties and Dynamics of Cold Atoms Moving through an Evanescent Wave¹

R. J. C. Spreeuw, V. V. Ivanov, R. A. Cornelussen, and H. B. van Linden van den Heuvel

Van der Waals–Zeeman Institute, University of Amsterdam, 1018 XE Amsterdam, The Netherlands

e-mail: spreeuw@science.uva.nl

Received October 19, 2004

Abstract—Measurements of the radiative properties of cold ⁸⁷Rb atoms close to a dielectric/vacuum interface are reported. This is the first observation of a quantum-electrodynamic (QED) modification of radiative properties in vacuum near a dielectric surface. Evanescent wave (EW) spectroscopy on cold atoms that were dropped on a glass surface was used. An increase of the natural linewidth by up to 25% compared to the free space value was found. This was attributed to QED broadening and level shifts, as well as local Stark shifts near the surface. By varying the characteristic EW length, a position dependence characteristic for QED was observed. The role of transient internal dynamics of the atoms as they move through the strongly inhomogeneous EW was investigated. © 2005 Pleiades Publishing, Inc.

INTRODUCTION

There is presently a large interest in (cold) atoms near surfaces. Examples include experiments on optical dipole traps near surfaces [1], experiments on atom chips [2, 3], and erbium-doped photonics [4]. Consequently, it is important to have a good understanding of the optical properties of cold atoms near surfaces.

Among the most remarkable effects caused by the surface are quantum-electrodynamic (QED) changes in the radiative linewidth and transition frequencies. The notion that the rate of spontaneous emission by an excited atom (or molecule) is not an intrinsic property of the atom but also depends on the environment was put forward by Purcell [5]. The spontaneous emission rate is proportional to the density of electromagnetic field modes (or “density of states” (DOS)), which can be influenced through the electromagnetic boundary conditions. At sufficiently small distances, the boundary conditions imposed by the environment not only change the radiative linewidth but also induce energy level shifts and thus change the transition frequencies. These include the electrostatic or van der Waals shift, the Casimir–Polder shift (a modification of the Lamb shift), and resonant radiative shifts. For a review, see, e.g., [6].

Modified spontaneous emission was first observed by Drexhage [7, 8] in dye monolayers separated from an interface by fatty acid layers. Both inhibited and enhanced spontaneous emission have since then been observed by others in a variety of geometries and circumstances [4, 9–11]. The radiative linewidth of an atom in vacuum at a distance of the order of an optical wavelength from a dielectric surface has never been

investigated experimentally. Energy level shifts have been studied for atoms inside cavities [12, 13] and in vapor cells, using selective reflection spectroscopy [14, 15]. The situation of an atom in front of a distant mirror has recently been investigated using a single trapped ion. Both the broadening of the radiative linewidth and energy level shifts have been reported for this system [16, 17].

Here we report on our experimental investigation of the radiative properties of cold ($T \approx 10 \mu\text{K}$) atoms of ⁸⁷Rb close to a glass surface, at a distance on the order of an optical wavelength. We have used our method of evanescent wave spectroscopy [1] to observe linewidth broadening with contributions from both QED broadening and level shifts. We compare our experimental results to a numerical analysis of the transient internal dynamics of an atom moving through the evanescent wave by a numerical integration of the time-dependent Bloch equations.

EXPERIMENT

Method: Evanescent Wave Spectroscopy

Both QED modification of the radiative linewidth and energy level shifts are significant mainly at distances $z \lesssim \chi = \lambda/2\pi$, where λ is the wavelength of the dominant electronic transition. In our case, this is the D_2 resonance line of Rb, and $\chi = 124 \text{ nm}$.

The radiative linewidth Γ is proportional to the local density of field states (DOS) at the position of the atom [18]. The electromagnetic boundary condition imposed by a dielectric surface changes the DOS, leading to a modification of Γ [4, 18–20] and to energy level shifts [14, 15, 20, 21].

¹ The text was submitted by the authors in English.

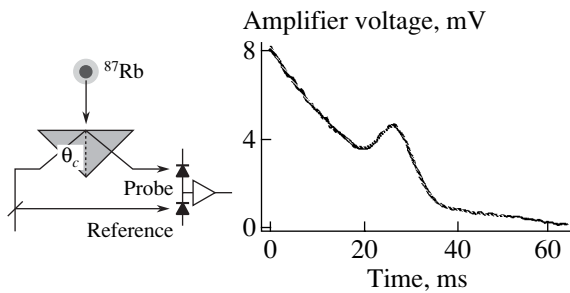


Fig. 1. The left figure shows the scheme of the experiment. Cold ^{87}Rb atoms are dropped on the surface of a glass prism. A weak evanescent wave probe beam is reflected from the prism surface and collected on a photodiode. A second photodiode collects light from a reference beam and the difference photocurrent is amplified, typically a fraction of 10^{-3} – 10^{-4} of the probe. On the right, a typical time-of-flight signal is shown ($100\times$ average). The peak is due to the absorption of evanescent probe light by cold atoms arriving at the surface. The signal has been distorted by AC coupling and is superposed on an exponentially decaying transient ($1/e$ time 26 ms).

Because the effects under study occur at very short range from the surface, we probe the cold atoms using evanescent wave (EW) spectroscopy [1]. This method is selectively sensitive to atoms very close to the surface due to the characteristic decay length of the EW. Our probe laser beam undergoes total internal reflection at the glass surface with index of refraction $n = 1.51$ (Fig. 1). The optical field on the vacuum side decays exponentially with the distance z to the surface, $E(z) \propto \exp(-z/\xi)$. Atoms can absorb light from the EW if their distance to the surface is on the order of the decay length $z \lesssim \xi \sim \lambda$.

The distance scale at which we probe can be adjusted because the EW decay length depends on the angle of incidence θ : $\xi(\theta) = \lambda(n^2 \sin^2 \theta - 1)^{-1/2}$. By increasing θ further above the critical angle $\theta_c = \arcsin n^{-1}$, the absorption will occur closer to the surface, where broadening and level shifts are more pronounced.

Experimental Setup

The major part of our experimental setup has been described previously [22]. Clouds of cold ^{87}Rb atoms are produced using magneto-optical trapping (MOT) and optical molasses, yielding about 3×10^7 atoms, at a temperature of 9 μK , corresponding to a Doppler width of 90 kHz (full width at half maximum; FWHM). By switching off the lasers, we drop the atoms on the surface of a glass prism, about 3.6 mm below the trap. After 27 ms, the atoms hit the surface, after a brief interaction with a weak, p -polarized, EW probe beam (Fig. 1). On their way down to the surface, the atoms can scatter photons out of the EW probe, so that a photodiode recording the probe power receives less power.

Since the missing fraction is typically 10^{-3} – 10^{-4} , we subtract the photodiode signal from a constant reference beam. The difference photocurrent is amplified using a low-noise current amplifier, resulting in a time-of-flight signal as shown on the right of Fig. 1.

As the probe, we use a home-built diode laser system. In order to avoid power broadening, we keep the intensity of the probe well below the saturation intensity. Using 0.35 μW and a waist of about 1 mm, the maximum saturation parameter was $s \approx 0.08$. The probe laser is locked to the $F = 2 \rightarrow F' = (1, 3)$ crossover resonance in the D_2 line of ^{87}Rb (780 nm) and shifted near resonance with the $F = 2 \rightarrow F' = 3$ transition using an acousto-optic modulator (AOM). By varying the AOM frequency, we tune the probe laser across the resonance and measure an absorption profile as a function of detuning.

Results and Data Processing

The time-of-flight signal at the output of the amplifier has a Gaussian time dependence. The signal shown in Fig. 1 has been distorted by AC coupling to the oscilloscope. This was done to suppress drifts on the photocurrent. Since the step response is known, we can fit a known function to the time-of-flight signal and extract the width and amplitude of the original Gaussian.

The Gaussian width is essentially constant. It is determined by the size of the atom cloud, its temperature, and its velocity as it reaches the surface. The amplitude of the Gaussian time-of-flight signal is proportional to the atom density and to the number of scattered photons per atom. We monitor the MOT fluorescence to normalize for shot-to-shot density fluctuations, although we find it to be essentially constant. We also monitor the probe power and normalize our signal to it since the absorbed power is also proportional to the probe power. For Fig. 1, the height of the peak is ~ 2 mV, which corresponds to an absorbed power of ~ 80 pW. The time-integrated signal amounts to $\sim 3 \times 10^6$ absorbed photons, or ~ 2 scattered photons per atom in the center of the EW probe. In the wing of the resonance or for large angles of incidence, this number drops to well below one scattered photon per atom.

By measuring the height of the Gaussian for a fixed angle of incidence and varying the probe detuning, we obtain an absorption profile as shown in Fig. 2. Far from the surface, the absorption profile is a Lorentzian with the natural linewidth $\Gamma_\infty/2\pi = 6.07$ MHz (FWHM) of the excited $5P_{3/2}$ state of Rb. At a distance z from the surface, this Lorentzian has a different linewidth $\Gamma(z)$ and a shifted central frequency $\omega_{eg}(z)$. The EW probe performs a convolution of the z -dependent Lorentzians with the exponential energy density of the EW, $U(z) \propto (-2z/\xi)$. As a result, the absorption profile is no longer Lorentzian. In practice, however, the change in the line shape is sufficiently small that we can still assign a Lorentzian width to it.

We do this by fitting a Voigt profile to the measured profile. This is the convolution of a Gaussian with a fixed width of 1 MHz (root-mean-square) and a Lorentzian with variable width. The fixed Gaussian linewidth accounts for the finite spectral width of the probe laser. We determined the laser linewidth in a separate measurement by observing the beat note between two similar but independently locked diode lasers on a photodiode.

The Lorentzian linewidth Γ contained in the Voigt profile is a fit parameter. In Fig. 3, we show the results for the fitted linewidths. Measurements for two different angles of incidence, $\theta - \theta_c = 0.16^\circ$ and 0.52° , are presented. The vertical error bars are determined by the scatter of the data points on the absorption profile. The data points at $\theta - \theta_c = 0$ correspond to the limit of large EW decay length, $\xi \rightarrow \infty$. Since this limit is very difficult to access experimentally, these data points have been measured using atoms in free space. We used the same probe laser to measure the absorption by the atomic cloud while falling, at a height of 2 mm above the surface. A short flash of probe light was recorded on a CCD camera and the absorption was determined from the camera image of the shadow of the cloud. The detuning was varied and the linewidth was again determined by fitting a Voigt profile.

COMPARISON WITH THEORY

We will now compare the measured θ dependence of the linewidth to QED calculations. When the atom approaches the dielectric surface, both the radiative linewidth Γ and the resonance frequency change in a z -dependent way. The latter also appears as a broadening in the experiment because the evanescent wave performs an integration over z . The absorption from the EW probe beam can be calculated by integrating the photon scattering rate over the vacuum half space $z > 0$. The photons that are scattered out of the EW by atoms are missing from the reflected probe beam so that the reflectivity drops below unity. This approach works well if the absorption is small ($\ll 1$).

We calculated the amount of photon scattering by two different methods. The first method is based on numerical integration of the optical Bloch equations (OBEs). As the falling atoms move through the EW, they encounter an increasing Rabi frequency and a position-dependent laser detuning due to the energy level shifts. The internal dynamics of the atom can therefore be rather complicated. The second calculation is based on the steady-state solution of the OBEs at each point along the atom's trajectory toward the surface.

Only the first method can fully take into account the transient internal dynamics and its possible effects on the observed linewidth. Note that such transients would at least qualitatively have the observed signature of a

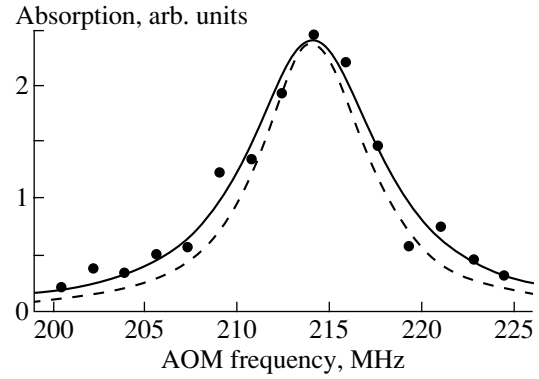


Fig. 2. Measured and fitted absorption profiles. The AOM frequency is the shift imparted to the frequency of the locked probe laser to tune it near resonance. Each data point is the fitted Gaussian amplitude of a $100\times$ averaged time trace, as in Fig. 1. The solid line is the fitted Voigt profile. For comparison, the dashed line shows the calculated free space Lorentzian profile.

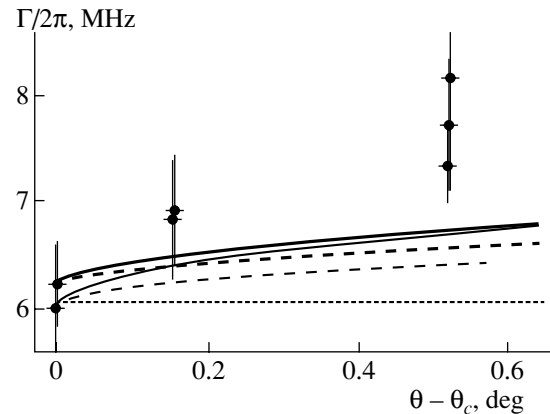


Fig. 3. Fitted linewidths for varying angle of incidence of the evanescent wave (EW) probe. The data points at $\theta - \theta_c = 0$ have been measured in free space instead of with an EW probe. The thin lines are the calculated widths based on Eq. (7), and the thick lines are based on an integration of the optical Bloch equations (see text). The dashed curves show the result when level shifts are not taken into account, while the solid curves take into account both broadening and level shifts.

broadening that increases with a decreasing EW decay length (increasing angle of incidence).

Bloch Equation Analysis

The first step is to calculate the perpendicular motion of the atom $z(t)$ in the potential near the surface. For the energy level shift of the ground $5S_{1/2}$ ($F = 2$) state, we take the expression from [21], using spectroscopic information from [23]. We multiply their result by $(n^2 - 1)/(n^2 + 1)$ because our surface is a dielectric instead of a mirror. This potential curve is shown in

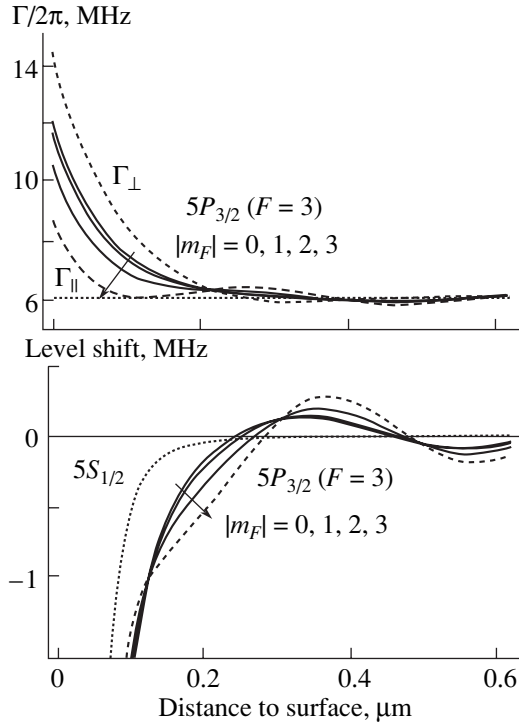


Fig. 4. Distance dependence of linewidths (upper) and level shifts (lower) of the relevant hyperfine magnetic sublevels. In the upper graph, the dashed curves show the dipole damping rates Γ_{\parallel} and Γ_{\perp} . The curves for the $F = |m_F| = 3$ states coincide with that for Γ_{\parallel} and do not contribute in the experiment. The dotted line is the free space value. In the lower graph, the level shifts of the $F = |m_F| = 3$ states do not contribute and are again shown as dashed.

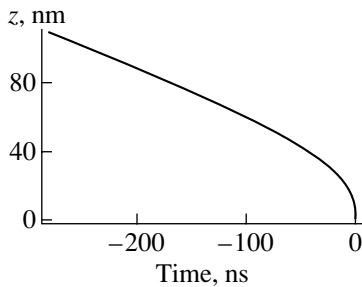


Fig. 5. Vertical motion of an atom in the accelerating ground state potential induced by the surface. The incident velocity is -0.26 m/s.

Fig. 4. The m_F sublevels have identical shifts. Very close to the surface, $z \lesssim \lambda$, the potential is dominated by the van der Waals potential $-C_3^g/z^3$.

We write the ground state potential as $V_g(z)$ and the velocity at which the atom enters the EW as $v_i < 0$. The velocity at a given height $v(z)$ is fixed by energy con-

servation, $m v^2(z)/2 + V_g(z) = m v_i^2/2$. The motion of the atom is then found by solving the differential equation

$$\dot{z} = v(z) = v_i \sqrt{1 - 2V_g(z)/m}. \quad (1)$$

In Fig. 5, we show the numerical solution of this equation of motion for $v_i = -0.26$ m/s and $z(0) = 0$.

The internal dynamics in the EW are governed by the OBEs. The falling atoms are in a mixture of all five magnetic sublevels $|F = 2, m_F\rangle$. The EW probe is p -polarized; i.e., the polarization is approximately linear, perpendicular to the surface. We make the approximation of treating every pair of levels $\{|F = 2, m_F\rangle, |F' = 3, m_F\rangle\}$ as a two-level system; i.e., we neglect effects of optical pumping during the transit through the EW.

The input parameters for the OBEs are the Rabi frequency Ω , the laser detuning δ_L , and the radiative linewidth Γ . All three change in a known z -dependent way. Since we have already solved the motion $z(t)$ of the atom, the z -dependent input parameters of the OBEs can now be written in time-dependent form, $\Omega(t) = \Omega(z(t))$, and similarly for Γ and δ_L . The OBEs for the pair of levels $\{|F = 2, m_F\rangle, |F' = 3, m_F\rangle\}$ now take the following form [24]:

$$\dot{u} = \delta_m(z(t))v - \frac{\Gamma_m(z(t))}{2}u, \quad (2)$$

$$\dot{v} = -\delta_m(z(t))u - \Omega_m(z(t))w - \frac{\Gamma_m(z(t))}{2}v, \quad (3)$$

$$\dot{w} = \Omega_m(z(t))v - \Gamma_m(z(t))w - \frac{\Gamma_m(z(t))}{2}. \quad (4)$$

The Rabi frequency is proportional to the electric field amplitude, decaying exponentially with distance to the surface, $\Omega_m(z) = \Omega_{m,0} \exp(-z/\xi)$.

The detuning changes due to energy level shifts close to the surface, $\delta_m(z) = \delta_L + V_g(z) - V_m(z)$. Here $\delta_m(z)$ denotes the detuning for the $|F = 2, m_F\rangle \rightarrow |F' = 3, m_F\rangle$ transition, δ_L is the laser detuning far from the surface, and $V_m(z)$ denotes the shift of the $|F' = 3, m_F\rangle$ magnetic sublevel. The shift of the ground $5S_{1/2}$ state $V_g(z)$ is dominated by the van der Waals shift $-C_3^g/z^3$. The shift of the excited $5P_{3/2}$ ($F' = 3, m_F$) states is more complicated, containing also a resonant component with oscillatory z dependence. We have used expressions for the shifts of both the ground and the excited states from [21], using transition line strengths taken from [23]. We have extended the expressions from [21] to account for the hyperfine structure. Furthermore, we have multiplied the results by a factor $(n^2 - 1)/(n^2 + 1)$ because our surface is a dielectric instead of a mirror. This is correct in the nonretarded limit [25], which

yields the dominant contribution in the experiment. The excited state level shifts $V_m(z)$ are shown in Fig. 4.

The modification of the radiative linewidth $\Gamma(z)$ near a dielectric surface has been described theoretically in terms of dipole damping rates Γ_\perp and Γ_\parallel [18, 19]. The subscripts \perp, \parallel refer to dipoles oriented perpendicularly and parallel to the surface, respectively. We calculate the variation of $\Gamma_\perp(z)$ and $\Gamma_\parallel(z)$ with the distance to the surface z using expressions given in [19].² The curves are shown in Fig. 4.

In our experiment, we probe ^{87}Rb atoms on the transition $5S_{1/2} (F = 2) \rightarrow 5P_{3/2} (F = 3)$. An atom in the excited magnetic hyperfine state $|F, m_F\rangle = |3, m\rangle$ can decay to the ground state $|2, m - q\rangle$ with $q = 0, \pm 1$. Choosing the quantization axis perpendicular to the surface, the $q = 0$ decay channel is governed by Γ_\perp , and the $q = \pm 1$ channels by Γ_\parallel . The decay rate for a given sublevel $|3, m\rangle$ is then given by

$$\Gamma_m(z) = c_{m,0}\Gamma_\perp(z) + (c_{m,-1} + c_{m,1})\Gamma_\parallel(z), \quad (5)$$

where $c_{m,q}$ is shorthand for the square of a Clebsch-Gordan coefficient, $c_{m,q} = \langle 2, m - q, 1, q | 3, m \rangle^2$. Note that this implies that close to the surface the m states have different lifetimes [19]. The different $\Gamma_m(z)$ curves are also shown in Fig. 4. Note that the curve for $|m| = 3$ is not relevant in our experiment because our p -polarized probe does not excite these m states.

We numerically solve the OBEs choosing as the initial condition that the atom is in the ground state at a large negative time: $u(t_0) = v(t_0) = 0$, $w(t_0) = -1/2$, where $\Gamma_\infty t_0 = -1000$. We then numerically integrate the OBEs until $t = 0$. A typical example of the solution is shown in Fig. 6. From this solution, we obtain the number of photons scattered by the atom on its way down to the surface by integrating $\int \Omega(t) v(t) dt$ [24]. We average this quantity over the different m states and vary the laser detuning δ_L over the absorption resonance. This yields an absorption profile, to which we fit a Lorentzian profile. Finally, the resulting Lorentzian linewidth is determined for different values of the EW decay lengths (angles of incidence). The final result is plotted together with our experimental data points in Fig. 3.

From the figure, we see that the Bloch equation calculation predicts only approximately half the linewidth broadening that is observed in the experiment. For comparison, we have also plotted the predicted linewidth if we do not take into account level shifts but only QED broadening. Clearly, the contributions of QED broadening and level shifts to the linewidth are very comparable and they should both be taken into account.

² Note that there appears a printing error in Eq. (58) of [19]; the coefficients $\rho^p(u)$ and $\rho^s(u)$ have been interchanged.

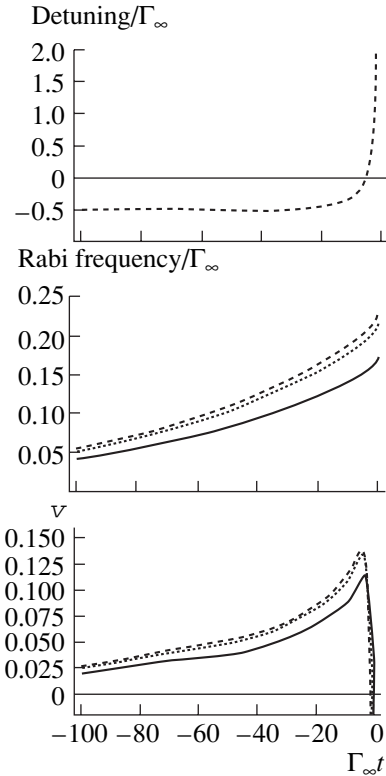


Fig. 6. Top: time-dependent detuning for $\delta_L/\Gamma_\infty = -0.5$, $\xi = 500$ nm. The curves for the different magnetic sublevels are indistinguishable on this scale. Middle: time-dependent Rabi frequency for the magnetic sublevels $|m_F| = 0, 1, 2$ (top down). Bottom: corresponding numerical solution for the v component of the optical Bloch equations. The three curves are for the magnetic sublevels $|m_F| = 0, 1, 2$ (top down).

Second Calculation; Spatial Integration

Our second calculation is based on a spatial integration of the photon scattering rate. In the limit of low saturation, the photon scattering rate is $\Gamma_m(z)c_{m,0}s_m(z)/2$, with the saturation parameter given by

$$s_m(z) = \frac{cU(z)}{I_0} \frac{\Gamma_\infty^2/4}{\delta_m^2(z) + \Gamma_m^2(z)/4}, \quad (6)$$

where $U(z) \propto \exp(-2z/\xi)$ is the EW energy density, $I_0 = 1.6$ mW/cm² is the (free space) saturation intensity, and c is the velocity of light in vacuum. Note that an increase in $\Gamma(z)$ not only increases the Lorentzian width but also multiplies into the photon scattering rate, thus increasing the on-resonance rate. This effect tends to favor the detection of atoms near the surface.

This approach of taking the local scattering rate proportional to the local saturation parameter implicitly assumes that the internal state of the atoms is given by the steady-state solution of the Bloch equations for the local values of $\Omega(z)$, $\delta_L(z)$, and $\Gamma(z)$. We integrate the photon scattering rate $\Gamma s/2$ over all $z > 0$. We repeat this

for each magnetic sublevel m because our ^{87}Rb atoms are in a random mixture of all five $|2, m\rangle$ states. The probe light is linearly polarized, perpendicularly to the surface, thus exciting $q = 0$ transitions.

Averaging over the m states, we arrive at the absorption of the probe, expressed as a fraction:

$$-\frac{\Delta P}{P} \propto \int \sum_{m=-2}^2 \frac{\Gamma_m(z) c_{m,0} \rho(z) e^{-2z/\xi}}{\delta_m^2(z) + \Gamma_m^2(z)/4} dz. \quad (7)$$

The atom density $\rho(z)$ is z -dependent due to the ground state level shift that accelerates the atoms to the surface. We take $\rho(z) = \rho_\infty v_i/v(z)$, with ρ_∞ being the density far from the surface. A good approximation is obtained using the van der Waals potential $V_g(z) = -C_3/z^3$, in which case the depletion of the density near the surface becomes $\rho(z) = \rho_\infty(1 + (z_W/z)^3)^{-1/2}$ with $z_W = (C_3^g/mgh)^{1/3} \approx 50$ nm.

Here $C_3^g = 5.6 \times 10^{-49}$ J m³ is the van der Waals coefficient and mgh is the kinetic energy with which the atoms fall onto the surface.

It is evident from Eq. (7) that the absorption profile is a convolution of Lorentzians with different widths, amplitudes, and central frequencies. The resulting absorption profiles are strictly speaking no longer Lorentzian. We have numerically calculated the expected absorption profiles using Eq. (7). In practice, the deviation from a Lorentzian is sufficiently small that we can fit a Lorentzian to the calculated profiles. The fitted widths are plotted in Fig. 3, together with the measured widths. In the same figure, we also show the result of the calculation if we do not take the level shifts into account. Again, the effect of the level shifts on the observed linewidth is comparable with the direct broadening effect.

DISCUSSION

Both the optical Bloch analysis and the steady-state analysis predict only about half the observed broadening of up to about 25%. The difference cannot be explained by obvious sources of spurious broadening. These include Doppler broadening (<2%), Zeeman broadening due to a spurious magnetic field (<3%), and power broadening (<0.5%). Furthermore, these broadening mechanisms would not show the observed signature of increasing with the angle of incidence. The calculation based on integration of the OBEs shows that transit time broadening cannot explain the difference either.

As a tentative explanation, we invoke the presence of local Stark shifts caused by charged or polarized particles on the surface. Based on a straightforward model calculation, we find that a surface charge density of $45e/\lambda^2$ yields a 10% linewidth increase. Remarkably, such a charge density corresponds to an average distance between the charges of the order of ~ 100 nm,

which is just the distance scale to which our experiment is very sensitive. Recently, McGuirk *et al.* have reported that Rb adsorbed on a Si or Ti surface generates local Stark shifts that are measurable as a change in the trapping frequency of their magnetic trap [26]. The authors mention that similar effects on a glass surface like ours are very small. However, there may be other charged or polarized adsorbates on the surface. Unfortunately, we have no detailed information about possible adsorbates to perform a more quantitative analysis. Our experiment is complementary to [26] in the sense that the latter measures a global effect, whereas our experiment is sensitive only to local variations of the electric fields.

CONCLUSIONS

In conclusion, we have observed a broadening of the natural linewidth of the D_2 resonance line of ^{87}Rb . This broadening was a combined effect of QED linewidth broadening and level shifts due to the proximity of a dielectric surface. The observed broadening of up to 25% was about twice that expected from theoretical calculations. The most plausible candidate for this discrepancy is the presence of local Stark shifts due to charged or polarized adsorbates on the surface.

ACKNOWLEDGMENTS

This work is part of the research program of the Stichting voor Fundamenteel Onderzoek der Materie (Foundation for Fundamental Research on Matter) and was made possible by financial support from the Nederlandse Organisatie voor Wetenschappelijk Onderzoek (Netherlands Organisation for Scientific Research).

REFERENCES

1. R. A. Cornelussen *et al.*, Eur. Phys. J. D **21**, 347 (2002).
2. R. Folman *et al.*, Phys. Rev. Lett. **84**, 4749 (2000).
3. J. Reichel, Appl. Phys. B **75**, 469 (2002).
4. E. Snoeks, A. Legendijk, and A. Polman, Phys. Rev. Lett. **74**, 2459 (1995).
5. E. Purcell, Phys. Rev. **69**, 681 (1946).
6. E. A. Hinds, Adv. At. Mol. Opt. Phys. Suppl. **2**, 1 (1994).
7. K. H. Drexhage, J. Lumin. **1-2**, 693 (1970).
8. K. H. Drexhage, in *Progress in Optics XII*, Ed. by E. Wolf (North-Holland, Amsterdam, 1974), p. 163.
9. R. G. Hulet, E. S. Hilfer, and D. Kleppner, Phys. Rev. Lett. **55**, 2137 (1985).
10. D. J. Heinzen, J. J. Childs, J. E. Thomas, and M. S. Feld, Phys. Rev. Lett. **58**, 1320 (1987).
11. A. M. Vredenberg *et al.*, Phys. Rev. Lett. **71**, 517 (1993).
12. V. Sandoghdar, C. Sukenik, E. Hinds, and S. Haroche, Phys. Rev. Lett. **68**, 3432 (1992).
13. C. Sukenik *et al.*, Phys. Rev. Lett. **70**, 560 (1993).

14. M. Chevrollier, D. Bloch, G. Rahmat, and M. Ducloy, *Opt. Lett.* **16**, 1879 (1991).
15. H. Failache *et al.*, *Eur. Phys. J. D* **23**, 237 (2003).
16. J. Eschner, C. Raab, F. Schmidt-Kaler, and R. Blatt, *Nature* **413**, 495 (2001).
17. M. A. Wilson *et al.*, *Phys. Rev. Lett.* **91**, 213602 (2003).
18. H. Khosravi and R. Loudon, *Proc. R. Soc. London, Ser. A* **433**, 337 (1991).
19. J.-Y. Courtois, J.-M. Courty, and J. C. Mertz, *Phys. Rev. A* **53**, 1862 (1996).
20. S.-T. Wu and C. Eberlein, *Proc. R. Soc. London, Ser. A* **455**, 2487 (1999).
21. E. A. Hinds and V. Sandoghdar, *Phys. Rev. A* **43**, 398 (1991).
22. D. Voigt *et al.*, *C. R. Acad. Sci., Paris* **2 (IV)**, 619 (2001).
23. M. S. Safronova, C. J. Williams, and C. W. Clark, *Phys. Rev. A* **69**, 022509 (2004).
24. C. Cohen-Tannoudji, J. Dupont-Roc, and G. Grynberg, *Atom-Photon Interactions* (Wiley, New York, 1992).
25. C. Eberlein and S.-T. Wu, *Phys. Rev. A* **68**, 033813 (2003).
26. J. M. McGuirk, D. M. Harber, J. M. Obrecht, and E. A. Cornell, *Phys. Rev. A* **69**, 062905 (2004).